

Design of Microfabricated Inductors

Luca Daniel
dluca@riovista.eecs.berkeley.edu

Charles R. Sullivan
charless@eecs.berkeley.edu

Seth R. Sanders
sanders@eecs.berkeley.edu

University of California, Berkeley
Department of Electrical Engineering and Computer Sciences
Berkeley CA 94720 U.S.A.

Abstract— Possible configurations for microfabricated inductors are considered. Inductance can be set by adjusting permeability through control of anisotropy of a permalloy core, or via a patterned quasi-distributed gap. A design methodology based on a simple model is proposed. Analysis of secondary effects is also developed. A design example for a 5 MHz buck converter application is presented. A power density of 12.8 W/cm² is possible for an efficiency of 94%.

I. INTRODUCTION

Recent advances in microfabrication of transformers, using thin-film magnetic materials, show much promise for miniaturization of power converters [1, 2, 3, 4, 5, 6, 7, 8, 9, 10, 11]. Microfabrication techniques can produce fine patterning and thin films, which are advantageous for the control of eddy current losses. This allows the use of magnetic metal alloys at frequencies in the range of 2-20 MHz. These materials can have high usable flux density and low hysteresis loss [9]. Although some inductors have been built using similar techniques [12, 13, 14, 4, 15, 16, 17, 18, 19, 20], many have not been designed for power applications. Through design and optimization specifically for these applications, higher efficiencies and power densities can be achieved.

In this paper, various geometries and fabrication methods for inductors are considered. Design calculations and optimizations for one configuration are developed. Specific results for an example design are presented.

II. INDUCTOR CONFIGURATIONS AND GEOMETRIES

The designer of a magnetic component with a magnetic core, fabricated by deposition of metal or other films on a substrate, faces a basic choice between depositing two layers of magnetic material with a conductor in between, or depositing two layers of conductor with a magnetic core in between. A device that uses two layers of conductor

Work supported by grants from National Semiconductor Corp. and the University of California Micro Program.

requires low resistance via contacts, and does not allow optimal use of an anisotropic magnetic material. As discussed in more detail in [9, 21], a configuration using two layers of magnetic material above and below a conductor is preferred for these reasons, and because it generally allows higher power density. This geometry has been applied in [10, 20].

A high-frequency inductor with substantial AC current requires careful design to avoid high AC conduction losses. Typical inductor designs for power applications include an air gap that can adversely affect the field distribution, inducing eddy currents, particularly with planar conductors and multi-turn windings. Perhaps the most elegant solution to this problem is the use of a low permeability magnetic material to act as a distributed gap across the top and the bottom of the conductors, as shown in Fig. 1. In

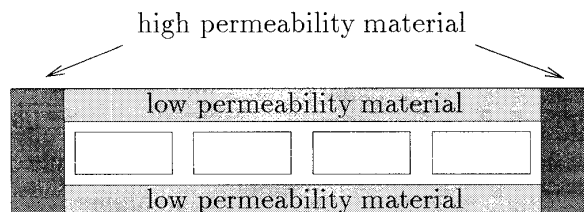


Fig. 1. Low permeability material acting as a distributed gap

this case, the field lines are nearly horizontal in the winding space, and the AC resistance effects are determined by the height of the conductor, not its width. Additionally, the number of turns does not affect AC resistance as long as the turns accumulate horizontally, rather than vertically [22, 9].

An approximation of this configuration can be fabricated as shown in Fig. 2, if a material with appropriate permeability is available. If it is necessary to use high-permeability materials, most designs will require increasing the overall reluctance of the magnetic path by intro-

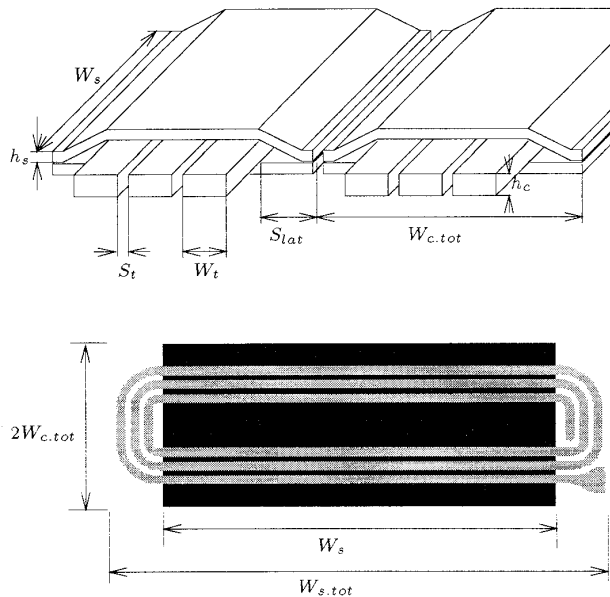


Fig. 2. Ungapped inductor configuration

ducing a gap. A series of fine gaps could be used to form a “quasi-distributed gap” to approximate a low permeability material [23, 9]. However, the scale of patterning that would be required for a typical design, on the order of one micron, would be difficult to achieve with a multilayer core [10]. Thus, discrete gaps are most easily placed at the “magnetic vias” where the top and bottom core materials connect. This leads to a large vertical field in the winding space, and problems with AC losses in the conductor. Turns that are wide compared to a skin depth, especially in multi-turn designs, become problematic. Designs that use single, narrow turns, such as the “meander coil” are preferred [10, 14, 24]. If the permeability required for an ungapped (i.e. distributed gap) design is achievable, the ungapped design is preferred.

III. CONTROL OF PERMEABILITY

A given permeability may be achieved in several different ways. A particular material or alloy may be selected to meet the requirements of a given design. Since this might require a new magnetic material deposition process for each design, a more practical approach would be to develop processes for a limited set of materials giving a range of permeabilities, and then adapt a design to match one of the available materials. A single material in which the permeability could be varied during deposition or by

other means would be even better.

Anisotropic materials such as permalloy (NiFe alloy) allow the possibility of controlling permeability through the application of a DC magnetic field in the easy-axis direction, while the inductor operates with the main flux path in the hard-axis direction. The applied field acts to increase the anisotropy energy, decreasing the permeability while maintaining the low hysteresis loss and high saturation flux density characteristics of the material. Control of permeability down to one eighteenth the zero-field permeability with an applied field of 22.6 Oe, has been demonstrated, as shown in Fig. 3. This has been proposed as a way to make devices with variable inductance, controlled by the applied field [15]. By applying a fixed field strength with a permanent magnet, it is possible, in principle, to use this as a method to set the permeability at the desired value for a given design.

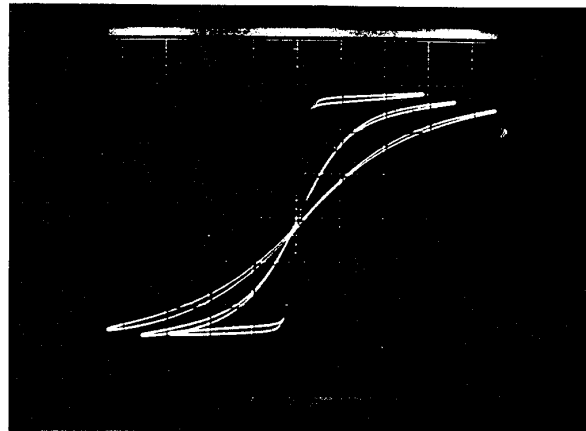


Fig. 3. Hard axis permeability controlled by an applied field: $\mu_r = 4300$ at zero-field; $\mu_r = 370$ with 9.9 Oe applied; $\mu_r = 230$ with 22.6 Oe applied.

IV. BASIC UNGAPPED DESIGN ANALYSIS

A design methodology is presented for an ungapped inductor, as in Fig. 2, to be used in a power converter circuit. A PWM buck converter is used as an illustrative example, but the calculations could be adapted for other converter topologies.

The optimization, presented in Appendix A, follows a procedure similar to that developed for a transformer design in [9]. In a first analysis the end turns, the lateral width S_{lat} needed to close the core, and the lateral separation S_t between turns have been neglected (see Fig. 2). A more detailed model will be presented in Section V to account for the effects of these factors.

First, the losses and power handling per unit area are calculated. The AC losses in the windings can be estimated, assuming a horizontal field in the window area, by a one dimensional analysis [25], and are found to depend only on the ratio between the height of the conductor h_c and the skin depth δ_c , even for multiple turns. This is described by an AC resistance factor $F_r(h_c) = R_{AC}/R_{DC}$.

If anisotropic NiFe alloy is used, and the main flux path is chosen along the non-hysteretic hard axis direction [9], only eddy currents will contribute to the loss in the core. To control this loss a laminated core, deposited as a multilayer film, can be used.

Finally, the throughput power density can be expressed as a function of the same parameters that determine the power loss.

A. Core optimization

The general guideline of the design will be the trade off between efficiency and power density. A given efficiency, for example, can be assigned during the design procedure and the power density then optimized.

According to the expressions in Appendix A, the power loss in the core can be made almost negligible by a large number of laminations, N . Given a fixed number of laminations, the height can be adjusted for maximum power density as shown in [9], yielding the expression

$$\frac{P_{out,opt}}{A} = \frac{34992\omega^2 B_{pk}^2 \rho_s^2 N^4}{3125\pi^6 (1-D)^6 \rho_c^2} \left[\frac{1-\eta}{\eta} \right]^5 \left[\frac{h_c}{1 + \frac{r^2 F_r(h_c)}{12}} \right]^3, \quad (1)$$

where ω is the operating frequency, ρ_s and ρ_c are the respective resistivities of the core and of the conductor, D is the duty cycle, h_c is the height of the conductor, F_r is the AC resistance factor, and $r = \Delta i_{pp}/I_{DC}$ is the ripple of the current. Variable B_{pk} is one-half the peak-to-peak value of the AC flux density. For an optimized design, the peak of total flux density should be close to (or at) the saturation level B_{sat} [9]. Hence, for our purposes, we design with $B_{pk} = B_{sat}/(1 + \frac{r}{2})$.

Designs optimized as described above correspond to a situation in which the power loss is distributed between core and winding such that

$$\frac{P_{coreloss}}{P_{windloss}} = \frac{2}{3}. \quad (2)$$

This relation holds in general for all optimized designs of planar inductors and transformers with the configuration in Fig. 2, as long as hysteresis losses are neglected, the core laminations are thin compared to a skin depth, and their number is decided a priori.

The optimal ratio (2) corresponds to the case where the height of the core is not constrained. In this case, the power density (1) of the device will increase with the

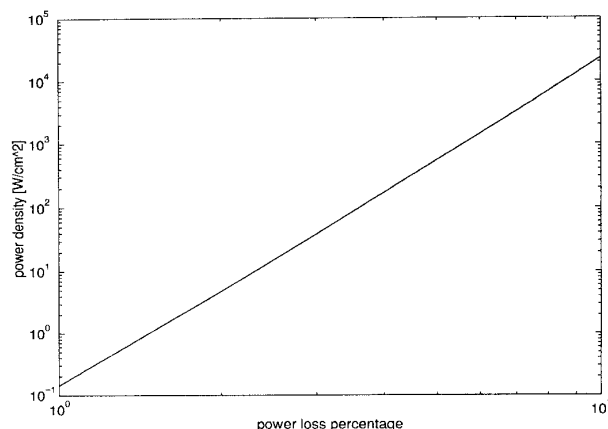


Fig. 4. Power density vs power loss percentage, for a fixed number of laminations $N = 12$. Parameters in Table I have been assumed. End turns and other second order effects have been neglected.

fourth power of the number of laminations. If, instead, the desired height of the core turns out to be too large to be practical, then a larger number of laminations will not significantly increase the power density, as shown in Fig. 5.

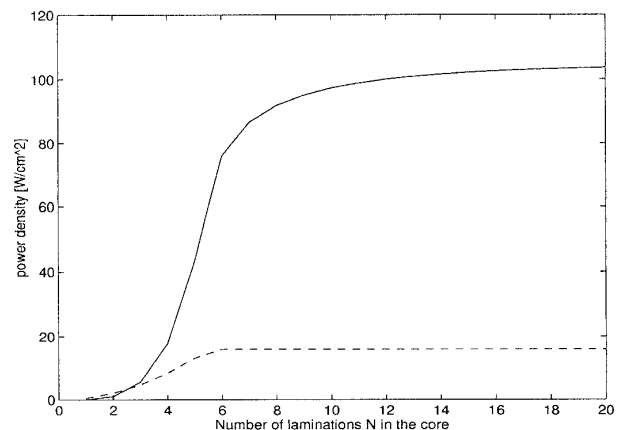


Fig. 5. The solid line shows the maximum power density at $\eta = 94\%$ vs. the number of laminations N . The dashed line shows the core height vs. number of laminations, limited at $16\mu\text{m}$. End turns and second order effects have been neglected.

B. Coil configuration and inductance adjustment

One way to satisfy the inductance requirement is by adjusting the permeability of the core as described in Section III. Besides giving a more favorable field configuration, this approach avoids the introduction of the induc-

tance constraint in the optimization process.

The optimum power density for a given efficiency (1) does not depend on the number of turns n . Therefore, one can design for a single-turn structure and then increase n to reduce the length/width aspect ratio. The flux carrying requirement specified by the application implies that the product $nW_s h_s$ is fixed. With this product fixed, the inductance

$$L = 2 \frac{n^2 \mu_0 \mu_r W_s h_s}{2nW_t}, \quad (3)$$

has no dependence on the number of turns n . Here, h_s is the core height, W_t is the width of a turn ($2nW_t$ is the magnetic path length), and W_s is width of the magnetic path (see Fig. 2). For the remainder of the paper, the dimension W_s will be referred to as the length of the core, because it corresponds to the longer dimension of the device.

The value of current density, $\sigma = I_{DC}/W_t$, required to attain a given efficiency, is calculated in the optimization process in Appendix A. This value can be achieved by choosing the width of each turn, W_t , according to the specified output current I_{DC} .

The effective permeability required to produce the desired inductance for the optimized design as calculated in Appendix B is given by

$$\mu_r(\eta) = \frac{2}{\mu_0 \sigma(\eta)} \left(\frac{B_{sat}}{1 + \frac{r}{2}} \right). \quad (4)$$

For an optimal design, $\mu_r(\eta)$ depends only on the chosen efficiency.

As an example, assuming the parameters in Table I and neglecting end-turn and other second order effects, designs in the range $96\% < \eta < 99\%$ are possible for values of relative permeability in the range $100 < \mu_r < 4000$, as shown in Fig. 6. Practical designs generally require higher permeability for a given efficiency, as they include the spaces to close the core S_{lat} and to separate the turns S_t , that increase the device width (see Fig. 2).

V. HEIGHT OF THE CONDUCTOR AND SECOND ORDER ANALYSIS

The optimization presented above does not specify the height of the conductor, h_c . As h_c is increased up to two skin depths, both AC and DC resistances decrease. Beyond this point, the improvement in AC resistance is small. With sufficient thickness, the DC loss can be made negligible in relation to AC loss. For higher values of h_c there will not be significant advantages because only the DC losses, already negligible, will be reduced.

When geometry considerations are also taken into account, increasing h_c will eventually make substantial the

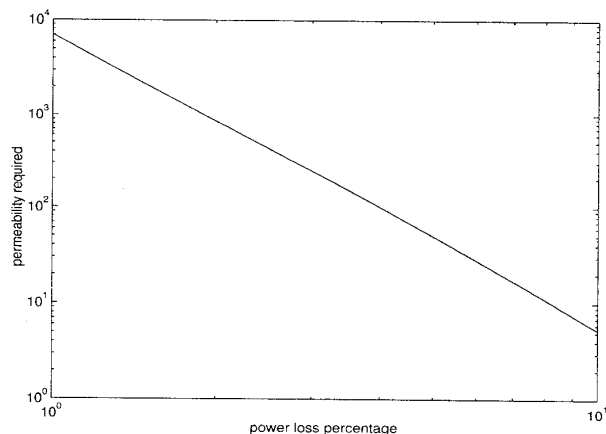


Fig. 6. Permeability versus power loss percentage for optimal design. Parameters in Table I have been assumed. End turns and second order effects have been neglected.

lateral width, S_{lat} , required to close the core and the lateral width, S_t , required to separate the turns. This effectively reduces the power density. Thus, the selection of conductor height h_c is a trade off between reducing resistance with a thicker conductor, or minimizing area by reducing S_{lat} and S_t with a thinner conductor.

A. End turns and secondary effects analysis

A more detailed model has been developed to take into account end-turn and other second order effects. Unitless factors have been introduced to account for these effects. The formulas presented in the basic analysis will then be modified only by multiplicative coefficients. The power loss in the end turns is captured by the factor K_{end} such that $R_{DC,tot} = R_{DC} K_{end}$. The factor K_s is defined such that $W_{s,tot} = W_s K_s$, where W_s is the length of the core (Fig. 2), and $W_{s,tot}$ is the total length of the device including end turns. Finally, K_c accounts for the width such that $W_{c,tot} = nW_t K_c$ where n is the number of turns and W_t is the width of each turn.

For many practical designs, where the width of a turn W_t is much larger than the height h_c , these factors are close to unity and the basic analysis presented above is a good approximation. However, for other designs, consideration of the factors K_{end} , K_s and K_c may be necessary to achieve an optimal design. The maximum power density for a given efficiency will now be reduced by the factor

$$\frac{1}{K_s K_c^3 K_{end}^3}, \quad (5)$$

as discussed in Appendix C. An iterative design or numerical optimization is necessary since these geometric factors depend on the dimensions of the device.

Because of these second order effects, the maximum achievable power density depends on the output current requirement. For small currents, the width occupied by conductors will be small compared to the total width of the winding area, which includes the lateral space S_{lat} to close the core. For this case, a large number of turns is preferred, limited by the increasing area and power loss added by the end turns. For a larger output current the width to close the core, S_{lat} , becomes small in relation to the width of the conductors W_t . In this case, a small number of turns is preferred, to minimize end-turn effects. If the device is then too long, it can be subdivided into several inductors connected in series, but located side-by-side. In conclusion, designs for higher output currents will have better performance than those for lower currents because of the reduced end turn effect and because the area needed to close the core and to separate the turns becomes negligible.

VI. EXAMPLE DESIGN

An example design for a PWM buck converter application [26] is presented to illustrate the design procedure. The circuit specifications can be found in Table I. A current ripple of 3A peak-to-peak over a DC current of 1A has been specified to achieve a zero-voltage-switching (ZVS) behavior. The operating frequency is limited by the power MOSFET characteristics. For a given efficiency, the power density of the inductor would increase with the square of the frequency as shown in expression (1). We outline the design procedure with the following steps. Final design parameters for our example are presented in Table I.

1. The curve expressing the maximum power density versus efficiency (Fig. 4) for a given number of laminations should be evaluated to choose an initial point for the design. For a first order design, the height of the conductor could be chosen as about one to two skin depths.
2. Expressions for the height of the core h_s and for the current density σ corresponding to the chosen efficiency can be found in Appendix A. If no satisfactory design point can be found, a higher number of laminations will have to be chosen. On the other hand, if the core thickness that results is too large, then the design may not take complete advantage of the high number of laminations (see Fig. 5).
3. The permeability required for the optimal design can then be calculated as shown in Appendix B.
4. The width of the conductor is determined by the current density and the specifications of the output current.

5. Given the height of the core h_s from step 1, the flux carrying requirement and the saturation level of the core determine the nW_s product, where n is the number of turns and W_s is the length of the core (Fig. 2). The number of turns can be used to adjust the length/width ratio of the device.
6. An iterative routine based on the model including end turns and second order effects presented in Appendix C can be used to refine the design (i.e., adjusting h_c) taking into account the second order effects. In our designs, we use a MathCad-based spreadsheet.

TABLE I
PARAMETERS OF EXAMPLE DESIGN

Symbol		Value
SPECIFICATIONS		
f	Frequency	5 MHz
I_{DC}	Output current	1 A
Δi_{pp}	Current ripple	3 A
V_{in}	Input voltage	40 V
V_o	Output voltage	5 V
D	Duty cycle	12.5 %
MATERIAL DATA		
B_{sat}	Saturation flux density	1.1 T
ρ_c	Conductor (Cu) resistivity	2 $\mu\Omega$ -cm
ρ_s	Core (80% NiFe) resistivity	20 $\mu\Omega$ -cm
μ_r	permeability required from design from ANSOFT simulations	367 208
DEVICE PARAMETERS		
N	Number of laminations in the core	12
h_s	Total height of core	16 μm
W_s	Length of the core	8.5 mm
B_{pk}	Peak of the flux density ripple	.54 T
L	Inductance required	292 nH
σ	current density	4 A/mm
W_t	Width of a single turn	250 μm
h_c	Height of conductor	40 μm
S_t	Width to separate each turn	40 μm
S_{lat}	Lateral width to close the core	500 μm
n	Number of turns	3
K_{end}	Factor for loss in end turns	1.29
K_s	Length factor	1.22
K_c	Width factor	2.50
PERFORMANCE		
R_{DC}	DC resistance from design from measurements	132m Ω 156m Ω
F_r	AC resistance factor from design from simulations	1.014 1.8
$P_{coreloss}$	Power loss in the core from design	103 mW
i_{max}	maximum current from design	2.5A
i_{sat}	current to saturate the core	2.8A
$W_{s,tot}$	Total length	10.8 mm
$2W_{c,tot}$	Total width	3.6 mm
	Output power	5 W
	Power density	12.8 W/cm ²
η	Efficiency from design	94 %

VII. PROCESS

A prototype implementing the example design is being fabricated. The process is similar to the one presented in [10, 11]. A silicon wafer is used as a substrate for com-

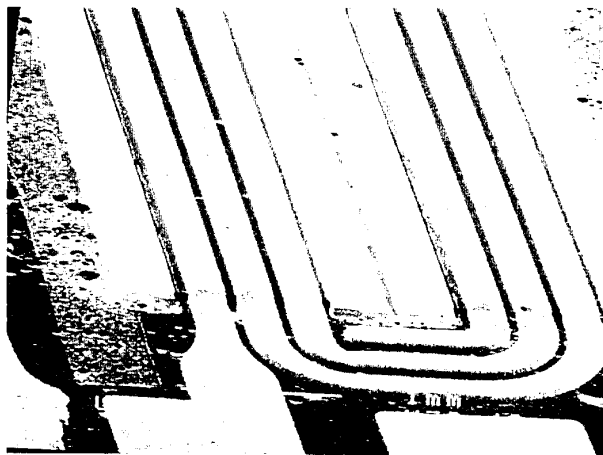


Fig. 7. SEM of the prototype fabricated in the Microlaboratory of the University of California at Berkeley.

patibility with IC technology. First a $2\ \mu\text{m}$ insulation layer of SiO_2 is deposited by low pressure chemical vapor deposition (LPCVD). The lower core laminations are then sputter-deposited using a multi-target system that allows switching easily from one layer to another. The 12 laminations of the NiFe permalloy (81% Ni) have an individual thickness of about $1.3\ \mu\text{m}$ and they are insulated by $0.3\ \mu\text{m}$ of SiO_2 . A very thin layer of Ti reinforces the adhesion. About 30 nm of chrome are then evaporated over the core, patterned and etched to constitute a mask for the core wet etch. A solution of hydrofluoric acid to attack the SiO_2 and nitric acid to attack the NiFe is used. The composition has been adjusted in order to have a slightly higher etch rate of the NiFe, so that the larger undercut will prevent short circuits between the laminations. In Fig. 8, the laminated core can be seen.

A $5\ \mu\text{m}$ layer of photoresist is then applied, patterned and hard baked to insulate the core from the coils. A thin layer of chrome (7 nm) and a seed layer of copper (200 nm) are evaporated. The copper seed layer is patterned, and the coil is then deposited by electroplating in a copper sulfate solution. The unpatterned chrome layer prevents the copper from growing beyond the copper seed layer. A rectangular current waveform at 100Hz and 80% duty cycle is used to help the plating process start uniformly on the copper and avoid the formation of dendrites. Finally, the chrome layer is removed with a sputter-etch process. Figs. 7 and 8 show the coil over the lower part of the core

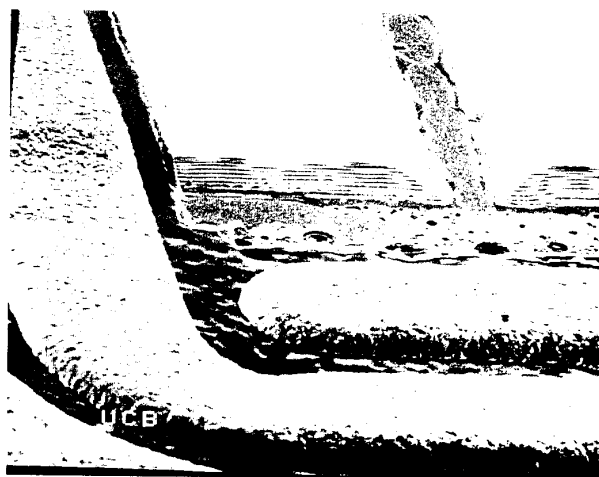


Fig. 8. Copper coils are electroplated over a laminated core. The core is composed of 12 laminations for a total thickness of $16\ \mu\text{m}$. Coils are $250\ \mu\text{m}$ wide and $40\ \mu\text{m}$ thick. The spacing between turns is $40\ \mu\text{m}$.

after the plating process.

The magnetic path will be closed by a lid applied on the top, built on a second silicon wafer. Bumps of hard baked photoresist, $60\ \mu\text{m}$ thick, under the sputtered laminations, will allow one to completely close the magnetic path when the lid is applied. Finally the required permeability will be obtained by putting a small permanent magnet over the upper wafer. ANSOFT simulations of the device being built (see Fig. 9) have been used to predict the value of the loss at the operating frequency $f = 5\ \text{MHz}$. The AC resistance factor from the simulation, assuming a lossless core, turned out to be $F_r = 1.8$. From the one dimensional analysis performed above a factor of $F_r = 1.014$ would have been expected. The difference can be explained by the reluctance of the side portions of the core, which are not constructed of higher-permeability material, as in Fig. 1.

On the same device a quasi-distributed gap configuration will also be attempted by the creation of several gaps along the upper part of the core. An ANSOFT simulation of a device with 3 gaps, each of them $12\ \mu\text{m}$ wide, positioned over each of the 3 turns (Fig. 10) gives an AC resistance factor $F_r = 1.8$, which promises performance close to that of the ungapped design.

VIII. STATUS OF EXPERIMENT

The fabrication of the lower wafer is complete and the feasibility of fabricating the upper wafer has been tested [11]. The DC resistance of the coils using a 4 point probe station, has been measured yielding a value of $156\ \text{m}\Omega$.

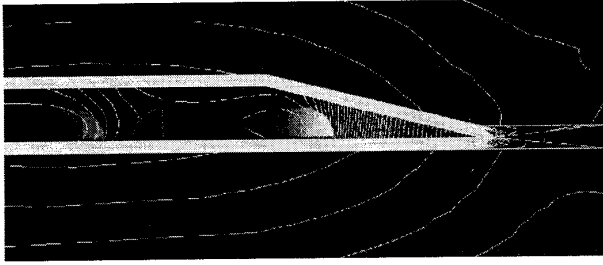


Fig. 9. ANSOFT simulation of the ungapped configuration. The dimensions are those indicated in the example design presented in Table I. The AC resistance factor results $F_r = 1.8$

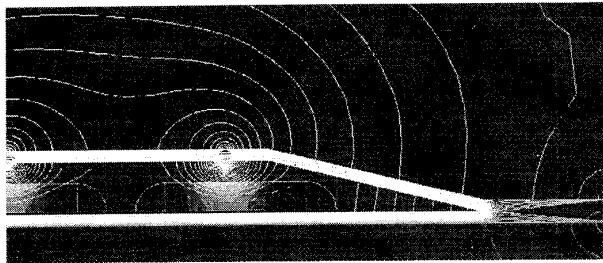


Fig. 10. ANSOFT simulation of the example design with 3 gaps on the upper lid core. Each gap is $12 \mu\text{m}$ wide. The AC resistance factor that results is $F_r = 1.8$.

The design value was $132 \text{ m}\Omega$. This discrepancy can be partially explained by the fact that the thickness of the coils in the measured device was $36 \mu\text{m}$ instead of $40 \mu\text{m}$. We also measured, with the same probe station, an inductance value of $L = 140 \text{ nH}$ at $f = 10 \text{ KHz}$ for the lower wafer, without the lid to close the magnetic path. ANSOFT simulations of this uncomplete structure predicted a value of $L = 103 \text{ nH}$ at the same frequency. The discrepancy is partially explained by the fact that the model for the simulation did not include the inductance due to the end turns.

IX. CONCLUSIONS

A methodology for design of microfabricated planar inductors to be used in a power conversion circuits has been presented. An example design for a 5 MHz buck converter shows that a power density of 12.8 W/cm^2 is theoretically possible with an efficiency of 94% . Simulations have confirmed an efficiency of 93% for such a device. The lower laminated core and the coils have been successfully fabricated. Coil DC resistance has been measured and found to be in reasonably good agreement with the design value.

APPENDIX

A. BASIC UNGAPPED DESIGN ANALYSIS AND OPTIMIZATION

First, the losses and power handling per unit area are calculated. End turns, space to insulate turns and space to close the core will be neglected in this analysis. Given these assumptions, the “active” area is

$$A = W_s 2nW_t. \quad (6)$$

See Fig. 2 and Table I for the meaning of the terminology. The loss in the windings per unit area due to the DC component can be estimated by

$$\frac{P_{windDC}}{A} = \frac{\frac{\rho_c 2nW_s}{W_t h_c} I_{DC}^2}{2nW_t W_s} = \frac{\rho_c}{h_c} \sigma^2, \quad (7)$$

where $\sigma = I_{DC}/W_t$ represents the current density per unit width of conductor.

The loss in the winding due to the AC component is approximated by the expression

$$\frac{P_{windAC}}{A} = \frac{\frac{\rho_c 2nW_s}{W_t h_c} F_r(h_c) I_{rms}^2}{2nW_t W_s} = \frac{r^2 F_r(h_c)}{12} \frac{\rho_c}{h_c} \sigma^2, \quad (8)$$

where $r = \Delta i_{pp}/I_{DC}$ represents the specified ripple factor of the triangular waveform of the current. Assuming a horizontal field in the winding area, the AC resistance factor $F_r(h_c) = R_{AC}/R_{DC}$ is estimated by

$$F_r(h_c) = 1 + \frac{5p^2 - 1}{45} \left(\frac{h_c}{\delta_c} \right)^4, \quad (9)$$

where $p = 1/2$ and δ_c is the skin depth of the conductor [25]. The total winding loss per unit area can then be written

$$\frac{P_{windloss}}{A} = \left[1 + \frac{r^2 F_r(h_c)}{12} \right] \frac{\rho_c}{h_c} \sigma^2. \quad (10)$$

Assuming laminations thinner than one skin depth and a sinusoidal flux density, the classical result in [27] is a good approximation for the loss in the core due to eddy currents. The hysteresis losses in the hard axis direction can be neglected and the total power loss in the core per unit area can then be estimated by the expression

$$\frac{P_{coreloss}}{A} = \frac{\omega^2 B_{pk}^2 h_s^3}{18 \rho_s N^2}. \quad (11)$$

The flux density has been assumed triangular and a sinusoidal waveform with the same rms value has been used for the estimation. For more precision, the loss due to each harmonic of the actual flux waveform could be calculated.

The throughput power density for a buck converter is

$$\frac{P_{out}}{A} = \frac{V_o I_{DC}}{A} = \frac{\Delta \lambda_{pp}}{T_{off}} I_{DC}, \quad (12)$$

where the output voltage has been expressed as a function of the off time T_{off} and the ripple in the flux linkage $\Delta \lambda_{pp}$. The latter can then be written as $\Delta \lambda_{pp} = 2n 2B_{pk} W_s h_s$, where $2B_{pk}$ is the peak-to-peak value of the flux-density ripple. In this way, the expression for the throughput power density becomes

$$\frac{P_{out}}{A} = \frac{\omega}{2\pi(1-D)} 2B_{pk} h_s \sigma, \quad (13)$$

where ω is the frequency and D is the duty cycle.

Next, the throughput power density is optimized for a given efficiency, as in [9]. The efficiency constraint imposed is

$$\frac{1-\eta}{\eta} \frac{P_{out}}{A} = \frac{P_{coreloss}}{A} + \frac{P_{windloss}}{A}, \quad (14)$$

and substituting the above expressions gives

$$\frac{1-\eta}{\eta} \frac{\omega}{2\pi(1-D)} 2B_{pk} h_s \sigma = \frac{\omega^2 B_{pk}^2 h_s^3}{18\rho_s N^2} + \left[1 + \frac{r^2 F_r(h_c)}{12} \right] \frac{\rho_c}{h_c} \sigma^2. \quad (15)$$

To facilitate calculations, this can be rewritten as

$$a\sigma^2 - bh_s\sigma + ch_s^3 = 0. \quad (16)$$

Solving for σ and choosing the largest current for largest power density

$$\sigma = \frac{h_s b}{2a} \left[1 + \sqrt{d(h_s)} \right], \quad (17)$$

where $d(h_s) = 1 - \frac{4ach_s}{b^2}$. Substituting in the power density expression (13), one finds

$$\frac{P_{out}}{A} = \left[\frac{\eta}{1-\eta} \right] \frac{b^2 h_s^2}{2a} \left[1 + \sqrt{d(h_s)} \right] \quad (18)$$

$$= \left[\frac{\eta}{1-\eta} \right] \frac{b^6}{32a^3 c^2} (1-d)^2 (1+\sqrt{d}). \quad (19)$$

Theoretically one optimizes for the best height of the core h_s , but in practice calculations are easier if d is calculated first. Setting to zero the derivative with respect to d of the expression above, the optimal value of d is found to be

$$d = \frac{1}{25}. \quad (20)$$

This means that the optimal core height is

$$h_{s,opt} = \frac{b^2}{4ac} (1-d) \quad (21)$$

$$= \frac{18\rho_s N^2 h_c (1-d)}{\rho_c \left[1 + \frac{r^2 F_r(h_c)}{12} \right] [2\pi(1-D)]^2} \left[\frac{1-\eta}{\eta} \right]^2, \quad (22)$$

which corresponds to a current density

$$\sigma_{opt} = \frac{18\omega B_{pk} \rho_s N^2 h_c^2 (1-d)(1+\sqrt{d})}{[2\pi(1-D)]^3 \rho_c^2 \left[1 + \frac{r^2 F_r(h_c)}{12} \right]^2} \left[\frac{1-\eta}{\eta} \right]^3. \quad (23)$$

Using these values, the maximum power density that results is

$$\frac{P_{out,opt}}{A} = \frac{34992\omega^2 B_{pk}^2 \rho_s^2 N^4}{3125\pi^6 (1-D)^6 \rho_c^3} \left[\frac{1-\eta}{\eta} \right]^5 \left[\frac{h_c}{1 + \frac{r^2 F_r(h_c)}{12}} \right]^3. \quad (24)$$

It can also be noticed that as

$$\frac{P_{coreloss,opt}}{A} = ch_s^3 = \frac{b^6}{64a^3 c^2} (1-d)^3, \quad (25)$$

and

$$\frac{P_{windloss,opt}}{A} = a\sigma^2 = \frac{b^6}{64a^3 c^2} (1+\sqrt{d})^2 (1-d)^2, \quad (26)$$

when the optimal design is achieved, the losses will be divided between core and winding such that

$$\frac{P_{coreloss,opt}}{P_{windloss,opt}} = \frac{(1-d)^3}{(1+\sqrt{d})^2 (1-d)^2} = \frac{2}{3}. \quad (27)$$

B. ESTIMATION OF THE PERMEABILITY REQUIRED TO PRODUCE THE DESIRED INDUCTANCE

Under the assumptions of the basic analysis where end-turn and second order effects have been neglected, the current density, $\sigma = I_{DC}/W_t$ is given for any efficiency as shown in Appendix A. For a closed core structure, with low reluctance via connections, this current density will then produce a field in the core equal to

$$H_{DC} = \frac{nI_{DC}}{2nW_t} = \frac{\sigma(\eta)}{2}, \quad (28)$$

which gives a flux density

$$B_{DC} = \mu_0 \mu_r \frac{\sigma(\eta)}{2}. \quad (29)$$

This flux density B_{DC} should be chosen in order to have the maximum value of the flux density correspond to the saturation level [9]. Therefore if r is the specified ripple of the current such that $\Delta I_{pp} = rI_{DC}$ then it should be true that

$$B_{DC} + \frac{rB_{DC}}{2} = B_{sat}, \quad (30)$$

which gives

$$B_{DC} = \frac{B_{sat}}{1 + \frac{r}{2}}. \quad (31)$$

The permeability should then be selected so that

$$\mu_r(\eta) = \frac{2}{\mu_0 \sigma(\eta)} \left(\frac{B_{sat}}{1 + \frac{r}{2}} \right). \quad (32)$$

C. ANALYSIS INCLUDING END-TURN AND SECOND ORDER EFFECTS

The analysis refers to the configuration in Fig. 2. The width to insulate each turn S_t and the width S_{lat} required to close the core can be assumed proportional to the height of the conductor. As an example, in our experimental fabrication process, $S_t = h_c$ and $S_{lat} = 12.5h_c$. The total DC resistance, including the end turns, can be estimated by the expression

$$R_{DC,tot} = \frac{\rho_c}{W_t h_c} 2nW_s \left[1 + \frac{4S_{lat} + \pi(W_t + S_t)n}{2W_s} \right] \quad (33)$$

$$= \frac{\rho_c}{W_t h_c} 2nW_s K_{end}, \quad (34)$$

which defines K_{end} .

The total length of the device can be estimated by the expression

$$W_{s,tot} = W_s + 2(W_t + S_t)n \quad (35)$$

$$= W_s \left[1 + \frac{2(W_t + S_t)n}{W_s} \right] = W_s K_s, \quad (36)$$

which defines K_s .

The total width of the device can be approximated by the expression

$$2W_{c,tot} = 2[nW_t + (n-1)S_t + 2S_{lat}] \quad (37)$$

$$= 2nW_t \left[1 + \frac{(n-1)S_t + 2S_{lat}}{nW_t} \right] = 2nW_t K_c, \quad (38)$$

which defines K_c .

The actual area occupied by the device can now be easily expressed as a function of these factors

$$A_{tot} = (W_s K_s)(2nW_t K_c). \quad (39)$$

The power loss in the core is modified as follows

$$\frac{P_{coreloss,tot}}{A_{tot}} = \frac{P_{coreloss}}{A} \frac{1}{K_s}. \quad (40)$$

An approximation for the total power loss in the windings can be written as

$$\frac{P_{windloss,tot}}{A_{tot}} = \frac{P_{windloss}}{A} \frac{K_{end}}{K_s K_c}. \quad (41)$$

Finally, the throughput power density that results is

$$\frac{P_{out,tot}}{A_{tot}} = \frac{P_{out}}{A} \frac{1}{K_s K_c}. \quad (42)$$

Following the optimization procedure presented for the basic analysis, the maximum power density for a given efficiency is found to be

$$\frac{P_{out,opt,tot}}{A_{tot}} = \frac{P_{out,opt}}{A} \frac{1}{K_s K_c^3 K_{end}^3}. \quad (43)$$

The optimal height of the core allowing this power density is now modified by the coefficient

$$h_{s,opt,tot} = h_{s,opt} \frac{1}{K_c K_{end}}. \quad (44)$$

The corresponding current density is modified to

$$\sigma_{opt,tot} = \sigma_{opt} \frac{1}{K_c K_{end}^2}. \quad (45)$$

The field in the core is

$$H_{DC,tot} = \frac{nI_{DC}}{2nW_t K_c} = \frac{\sigma_{opt,tot}}{2K_c}. \quad (46)$$

Following the calculations in Appendix B, the permeability required is found to be

$$\mu_{r,tot} = \frac{2}{\mu_0 \sigma_{opt,tot}} \left(\frac{B_{sat}}{1 + \frac{\pi}{2}} \right) K_c. \quad (47)$$

REFERENCES

- [1] Kiyohito Yamasawa, Kenji Maruyama, Isao Hirohama, and Paul Biringer. High-frequency operation of a planar-type microtransformer and its application to multilayered switching regulators. *IEEE Trans. on Magnetics*, 26(3):1204–1209, May 1990.
- [2] K. Yamaguchi, E. Sugawara, O. Nakajima, and H. Matsuki. Load characteristics of a spiral coil type thin film microtransformer. *IEEE Trans. on Magnetics*, 29(6):3207–3209, 1993.
- [3] Kazuyuki Yamaguchi, Shigehiro Ohnuma, Takao Imagawa, Jirou Toriu, Hidetoshi Matsuki, and Koichi Murakami. Characteristics of a thin film microtransformer with spiral coils. *IEEE Trans. on Magnetics*, 29(5):2232–2237, 1993.
- [4] M. Yamaguchi, S. Arakawa, H. Ohzeki, Y. Hayashi, and K. I. Arai. Characteristics and analysis for a thin film inductor with closed magnetic circuit structure. *IEEE Trans. on Magnetics*, 28(5), 1992.
- [5] T. Yachi, M. Mino, A. Tago, and K. Yanagisawa. A new planar microtransformer for use in micro-switching-converters. In *22nd Annual Power Electronics Specialists Conf.*, pages 1003–1010, June 1991.
- [6] T. Yachi, M. Mino, A. Tago, and K. Yanagisawa. A new planar microtransformer for use in micro-switching-converters. *IEEE Trans. on Magnetics*, 28(4):1969–73, 1992.
- [7] M. Mino, T. Yachi, A. Tago, K. Yanagisawa, and K. Sakakibara. Microtransformer with monolithically integrated rectifier diodes for micro-switching converters. In *24th Annual Power Electronics Specialists Conf.*, pages 503–508, June 1993.
- [8] M. Mino, T. Yachi, K. Yanagisawa, A. Tago, and K. Tsukamoto. Switching converter using thin film microtransformer with monolithically-integrated rectifier diodes. In *26th Annual Power Electronics Specialists Conf.*, pages 665–670, June 1995.
- [9] C. R. Sullivan and S. R. Sanders. Design of microfabricated transformers and inductors for high-frequency power conversion. *IEEE Trans. on Power Electronics*, 11(2):228–238, 1996.
- [10] C. R. Sullivan and S. R. Sanders. Microfabrication process for high-frequency power-conversion transformers. In *26th Annual Power Electronics Specialists Conf.*, pages 658–64, June 1995.
- [11] C. R. Sullivan and S. R. Sanders. Measured performance of a high-power-density microfabricated transformer in a dc-dc converter. In *27th Annual Power Electronics Specialists Conf.*, June 1996.
- [12] K. Kawabe, H. Koyama, and K. Shirae. Planar inductor. *IEEE Trans. on Magnetics*, 20(5):1804–1806, September 1984.
- [13] O. Oshiro, H. Tsujimoto, and K. Shirae. A novel miniature planar inductor. *IEEE Trans. on Magnetics*, 23(5):3759–3761, September 1987.
- [14] M. Yamaguchi, S. Arakawa, S. Yabukami, K. I. Arai, F. Kumagai, and S. Kikuchi. Estimation of the in-situ permeabilities in thin-film inductors. *IEEE Trans. on Magnetics*, 29(5), 1993.
- [15] Nabil Saleh. Variable microelectronic inductor. *IEEE Transactions on Components, Hybrids, and Manufacturing Technology*, CHMT-1(1), 1978.
- [16] M. Yamaguchi, M. Matsumoto, H. Ohzeki, and K. I. Arai. Fabrication and basic characteristics of dry-etched micro inductors. *IEEE Trans. on Magnetics*, 26(5), 1990.
- [17] Chong H. Ahn, Yong J. Kim, and Mark G. Allen. A fully integrated micromachined toroidal inductor with a nickel-iron magnetic core (the switched dc/dc boost converter application). In *7th Annual International Conf. on Solid-State Sensors and Actuators*, pages 70–73, 1993.
- [18] Chong H. Ahn and Mark G. Allen. A comparison of two micromachined inductors (bar- and meander-type) for fully integrated boost dc/dc power converters. *IEEE Trans. on Power Electronics*, 11(2):239–245, March 1996.
- [19] R. F. Soohoo. Magnetic thin film inductors for integrated circuit applications. *IEEE Trans. on Magnetics*, MAG-15(6):1803–1805, November 1979.
- [20] M. Mino, K. Tsukamoto, K. Yanagisawa, A. Tago, and T. Yachi. A compact buck-converter using a thin-film inductor. In *11th Annual Applied Power Electronics Conference and Exposition*, pages 422–426, March 1996.
- [21] C. R. Sullivan and S. R. Sanders. Microfabrication of transformers and inductors for high frequency power conversion. In *24th Annual Power Electronics Specialists Conf.*, pages 33–40, June 1993.
- [22] W. M. Chew and P. D. Evans. High frequency inductor design concepts. In *22nd Annual Power Electronics Specialists Conf.*, pages 673–678, June 1991.
- [23] Ulrich Kirchenberger, Michael Marx, and Dierk Schroder. A contribution to the design optimization of resonant inductors in high power resonant converters. In *1992 IEEE Industry Applications Society Annual Meeting*, volume 1, pages 994–1001, October 1992.
- [24] I. Sasada, T. Yamaguchi, and K. Harada. Methods for loss reduction in planar inductors. In *23rd Annual Power Electronics Specialists Conf.*, pages 1409–1415, June 1992.
- [25] P.L. Dowell. Effects of eddy currents in transformer windings. *Proceedings of the IEE*, 113(8):1387–1394, August 1966.
- [26] A. J. Stratakos, S. R. Sanders, and R. W. Brodersen. A low-voltage cmos dc-dc converter for a portable battery-operated system. In *25th Annual Power Electronics Specialists Conf.*, pages 619–626, June 1994.
- [27] E. C. Snelling. *Soft Ferrites, Properties and Applications*. Butterworths, second edition, 1988.